FLAT-FIELDING OF SOLAR Hα OBSERVATIONS USING RELATIVELY SHIFTED IMAGES

JONGCHUL CHAE
Astronomy Program, School of Earth and Environmental Science, Seoul National University, Seoul 151-742, Korea (e-mail: chae@astro.snu.ac.kr)

(Received 5 January 2004; accepted 29 January 2004)

Abstract. A new algorithm is proposed to determine the flat pattern from a set of relatively shifted images. It simultaneously searches for the flat pattern, the object image, the light levels, and optionally the relative displacements that optimize the sum of the error squares. We have applied the method to real Hα observations, and examined in detail the dependence of the accuracy of the solution on the iteration number, the light level change, the dither pattern, and the noise. It has been found that the method can produce a flat pattern with an error down to 0.25% of the mean level in Hα observations with low noise.

1. Introduction

An ideal imaging system should produce the image of an object whose data number is proportional to the intensity of the object only, and is independent of the detector position. In real situations the image recorded on the detector,

$$a = of + n, \tag{1}$$

reflects not only the image of the object o, but also the non-uniform response (commonly called 'flat pattern') f and the noise n (we suppose dark frame and bias have been already subtracted). Note that the non-uniform flat pattern is the combined effect of all the optical components of the observing instrument as well as the detector itself.

Flat-fielding is a process of determining the object image o from the observed image a. The most important step in flat-fielding is the determination of the flat pattern f. The simplest way of getting the flat pattern is to image a uniformly illuminated object. Twilight and dome are widely selected for this purpose in nighttime observations (e.g., Stetson and Harris, 1988). The major difficulty of this kind of approach is that the object is not uniform to a sufficient accuracy. It is known that the intensity of dome or twilight is uniform at best at the 1% level (Stetson and Harris, 1988). In high-resolution solar observations, the flat image is obtained by integrating a number of images taken while moving the telescope around a quiet-Sun area near disk center (e.g., Yang *et al.*, 2003). Even if this method is simple and very convenient, it cannot be applied to the case where the field of

Solar Physics **221:** 1–14, 2004.

view contains high contrast objects so that the image integration is not effective. Full-disk observations are such an example.

Dalrymple, Bianda, and Wiborg (2003) proposed a method of computing a flat field from two orthogonal constant-speed scans of an image across the detector. The strong point of this method is its fast speed. But the accuracy may not be high enough especially when the constancy of the scan speed during the exposure is not ensured.

An alternative approach is to construct the flat pattern from a set of relatively shifted images of a non-uniform object (Kuhn, Lin, and Loranz, 1991; Wild, 1997; Fixsen, Moseley, and Arendt, 2000). The algorithm of Kuhn, Lin, and Loranz (1991, hereafter KLL) is relatively simple and hence has been frequently applied to solar observations (e.g., Denker *et al.*, 1999). This method makes use of the property that the ratio of two images of the same object recorded on two different pixels is equal to the ratio of the gains between the two pixels. Therefore, it is possible to determine the pixel-to-pixel variation of the gain when two frames that are displaced with respect to each other are analyzed together. To ensure sufficient accuracy of the method, many pairs of frames may be used. The strongest point of this method is that it provides a very convenient way of determining the flat pattern even without uniform illumination. Moreover, the optical setup for obtaining the flat pattern is the same as that for main observations so that the determined flat pattern should be quite suited for main observations.

The KLL method, however, has a few shortcomings. As pointed out by the authors, the solution has a gauge freedom that may produce a linearly varying artifact-pattern. Especially when successive image frames do not have the same mean signal level, a large systematic error may arise. In addition, when many successive frames are used, the computing time increases drastically, which is proportional to the number of all possible combinations of two frames or to the square of the number of frames.

I propose a new method. Like the KLL method, my method uses a number of frames that image the same object on the different positions of the detector. But it does not take the ratio of two frames. Instead, the object image as well as the flat pattern is treated as a free parameter to be determined. Moreover, the light level that may vary from frame to frame is also treated as a free parameter to be determined. In addition we can treat the relative displacements between frames to be free parameters. The determination of the relative displacements and the shifting of images are all done to sub-pixel accuracy using interpolations. Summing up, my method simultaneously searches for the flat pattern, the object image, the light level, and optionally the relative displacements that optimize the sum of the error squares. The solution turns out to be much less subject to the shortcomings in the KLL approach.

2. Method

2.1. Formulation

Let i and j represent the row and column indices of a detector consisting of N_x by N_y pixels, and o_{ij} represent the ideal image of the object. Suppose we consecutively take N_f images of the same object with slightly different fields of view. Then the kth observed image a_{ij}^k may be mathematically modelled as

$$a_{ij}^k = c_k o_{i-x_k, j-y_k} f_{ij} + n_{ij}^k, \tag{2}$$

where x_k and y_k are the displacement of a_{ij}^k with respect to o_{ij}, f_{ij} the flat pattern, and n_{ij}^k the random additive noise. The parameter c_k has been introduced to take into account the light level variation that depends on the atmospheric condition and so on.

The logarithmic form of the above equation is

$$A_{ij}^k = C_k + O_{i-x_k, j-y_k} + F_{ij}, \tag{3}$$

where the capital letters represent the logarithms of the corresponding variables. We seek to determine C_k, O_{ij}, F_{ij} and optionally x_k, y_k by minimizing the functional

$$\chi^2 = \sum_{ijk} (C_k + O_{i-x_k, j-y_k} + F_{ij} - A_{ij}^k)^2 w(i - x_k, j - y_k), \tag{4}$$

where the new function w has been introduced to deal with the boundary effects, and is defined as

$$w(i, j) \equiv \begin{cases} 1 & \text{for} \quad 0 \le i \le N_x - 1 \ \text{ and } \ 0 \le j \le N_y - 1, \\ 0 & \text{otherwise.} \end{cases} \tag{5}$$

The functional may be also written as

$$\chi^2 = \sum_{ijk} (C_k + O_{ij} + F_{i+x_k, j+y_k} - A_{i+x_k, j+y_k}^k)^2 w(i + x_k, j + y_k) \ . \tag{6}$$

The minimization of the functional χ^2 based on the linearization requires determination of the gradient and the second derivative matrix (Hessian matrix) with respect to the free parameters. Note the Hessian matrix is a huge array of $(2N_x N_y + 3N_f)^2$ size, so that working with the full elements of this matrix is a formidable task. For tractability, we assume all the off-diagonal components of the matrix are negligibly small. Then we only have to calculate the $(2N_x N_y + 3N_f)$ diagonal components and the solution of the linearized equation is simply given by the gradient divided by the corresponding diagonal components of the matrix. We thus obtain the following formulae for the iterative solution:

$$\Delta F_{ij} \approx -\frac{\sum_k (C_k + O_{i-x_k, j-y_k} + F_{ij} - A_{ij}^k) w(i - x_k, j - y_k)}{\sum_k w(i - x_k, j - y_k)} \ , \tag{7}$$

$$\Delta O_{ij} \approx -\frac{\sum_k (C_k + O_{ij} + F_{i+x_k, j+y_k} - A^k_{i+x_k, j+y_k}) w(i + x_k, j + y_k)}{\sum_k w(i + x_k, j + y_k)} , \tag{8}$$

$$\Delta C_k \approx -\frac{\sum_{ij} (C_k + O_{i-x_k, j-y_k} + F_{ij} - A^k_{ij}) w(i - x_k, j - y_k)}{\sum_{ij} w(i - x_k, j - y_k)} . \tag{9}$$

When the improvement of the relative displacement (x_k, y_k) is necessary, it is possible to use the iterative formulae

$$\Delta x_k \approx -\frac{\sum_{ij} (C_k + O_{i-x_k, j-y_k} + F_{ij} - A^k_{ij}) w(i - x_k, j - y_k) \delta_i}{\sum_{ij} w(i - x_k, j - y_k) \delta_i^2}, \tag{10}$$

$$\Delta y_k \approx -\frac{\sum_{ij} (C_k + O_{i-x_k, j-y_k} + F_{ij} - A^k_{ij}) w(i - x_k, j - y_k) \delta_j}{\sum_{ij} w(i - x_k, j - y_k) \delta_j^2}, \tag{11}$$

with

$$\delta_i \equiv -\left.\frac{\partial O_{ij}}{\partial i}\right|_{i-x_k, j-y_k} \quad \text{and} \quad \delta_j \equiv -\left.\frac{\partial O_{ij}}{\partial j}\right|_{i-x_k, j-y_k} . \tag{12}$$

2.2. Starting values

Determination of the relative displacements of the images is crucial in our method. The frame taken at the middle of the sequence was chosen as the temporary reference and the relative displacement (x_k, y_k) of each image was determined with respect to this reference which maximizes the cross-correlation between the two. The cross-correlation function was calculated using the commonly adopted Fourier transform method, and the offset values were determined with sub-pixel accuracy based on five-point interpolation using the pixel of maximum cross-correlation and its four neighboring pixels. Once the relative displacements of all the images with respect to the temporary reference are determined, the reference is reset to a new reference by subtracting the average from (x_k, y_k).

When the contrast of the non-uniform detector pattern dominates the observed images, it is difficult to apply the cross-correlation technique to determine the relative displacements. In this case, we treat a rough flat-fielding before applying the cross-correlation. We find that the pre-flat-pattern constructed by taking the median of all the images at each pixel is good enough for this purpose.

Our choice of the other starting values is as follows:

$$F_{ij} = 0 , \tag{13}$$

$$O_{ij} = \sum_k A^k_{ij} / N_f , \tag{14}$$

$$C_k = \sum_{ij} A_{ij}^k/(N_x N_y) - \sum_{ij} O_{ij}/(N_x N_y) \ . \tag{15}$$

At this point I would like to mention that the final solution is not fully independent of the starting values. This means that the solution is not unique, and the choice of the starting values may be important. The nature and effect of this gauge freedom was well described by KLL. They found that this gauge freedom may introduce serious artifacts in the solution when the light level changes. As we shall see, the gauge freedom is not a big problem in the present approach since the light levels are self-consistently determined.

2.3. Posterior adjustment

There is a degeneracy among C_k, F_{ij} and O_{ij} by constant factors. For the uniqueness of the solution, we constrain C_k and F_{ij} to satisfy

$$\langle C \rangle \equiv \sum_k C_k/N_f = 0 \quad \text{and} \quad \langle F \rangle \equiv \sum_{i,j} F_{ij}/N_x N_y = 0 \ . \tag{16}$$

This constraint is easily fulfilled by adding the appropriate values to the determined C_k, F_{ij}, and O_{ij}.

2.4. Program implementation

The algorithm has been implemented in the Interactive Data Language (IDL). The program code is available from the author on request. Given fourteen images of 1024×1024 pixels, the computing time for 10 iterations was 160 s in a laptop computer equipped with the Intel Pentium M 1.6 GHz processor, Microsoft Windows XP, and the Interactive Data Language v6.0.

3. Application to Real Hα Observations

3.1. Hα −1.2 Å Observations

We took a set of images of a solar active region at the Hα −1.2 Å on 4 October 2003 using the Big Bear Solar Observatory 65-cm telescope. Using the fast CCD digital camera 1M30P made by the Dalsa company, 30 frames of 1024 by 1024 pixels were captured each second, but only the best one, selected with the technique of frame selection, was stored. Then we manually moved the telescope a little bit and took a new image that was shifted with respect to the previous one. This process was repeated until all of the 14 images were stored. Figure 1(a) shows one of the observed images A_{ij}^k . It took about 75 s to finish this observation.

Figure 1(b) and (d) are the flat pattern and the object image determined after 20 iterations using our method. Different kinds of features are easily recognized

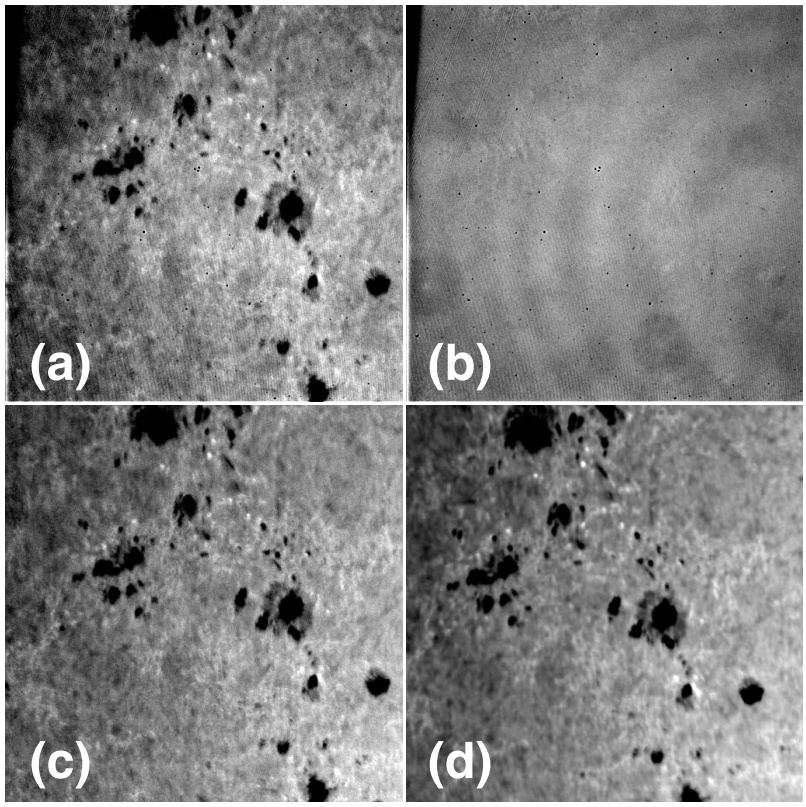

Figure 1. The logarithms of (a) one of the fourteen observed Hα $-$ 1.2 Å images A_{ij}^k, (b) the flat pattern F_{ij}, (c) the flat-field-corrected image $A_{ij}^k - F_{ij}$, and (d) the object image O_{ij}. The gray scale range is the median value $\pm$ 0.05.

in the flat pattern including ubiquitous dots, circle-like dust diffraction patterns, the low-frequency fringe pattern, and the high-frequency fringe pattern, the dark streak in the upper half portion of the left boundary that may be attributed to the field stop. These features are absent in the object image, and hence may be of purely instrumental origin.

Note the object image in Figure 1(d) is different from the flat-field-corrected image in Figure 1(c) in a couple of ways. They have slightly different fields of view. In addition, the object image has a higher signal-to-noise ratio than the raw image, for it has been constructed from all the raw images. Supposing that the object image is noise-free, we can estimate the noise in the flat field corrected image in Figure 1(c). It is found to be about 2.6% of the mean value.

We find that the root-mean-square contrast of the flat pattern, 3.4% of the mean value, is smaller than that of the object image (true pattern), 5.7%. Therefore, the true features are better identified in the raw image in Figure 1(a) than the flat

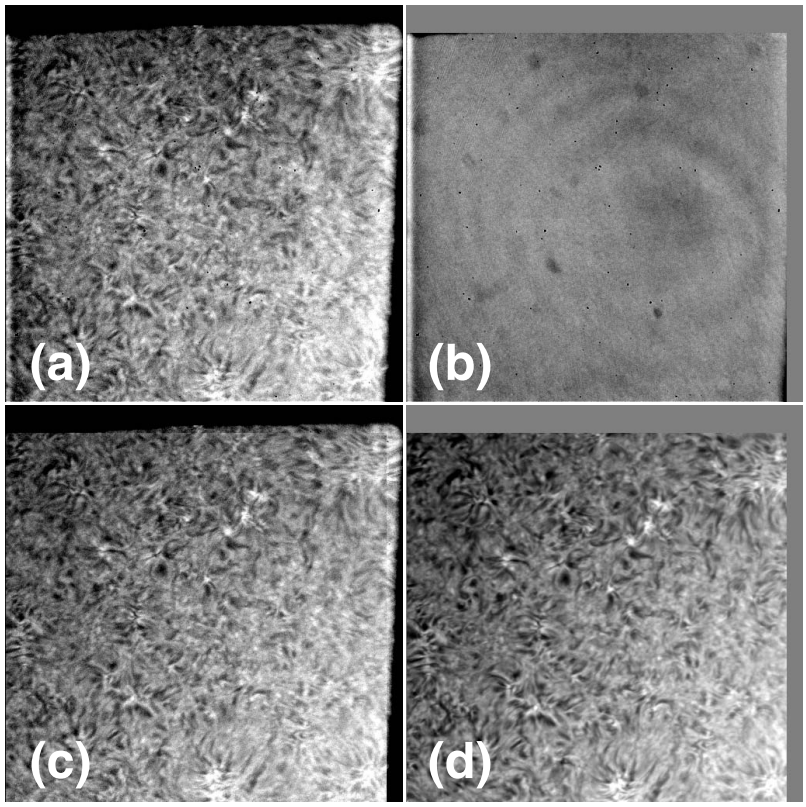

Figure 2. The logarithms of (a) one of the fourteen observed Hα centerline images A_{ij}^k, (b) the flat pattern F_{ij}, (c) the flat-field-corrected image $A_{ij}^k - F_{ij}$, and (d) the object image O_{ij}. The gray scale range is the median value $\pm$ 0.1.

pattern, and this is one reason why our determination of the displacements was successful.

We also find that the light level changes from frame to frame. The standard deviation of the fluctuation is found to be 1.3%. It is likely that the fluctuation is due to the time-varying seeing condition, which may be commonly encountered in the short-exposure observations. In the next section we will demonstrate that this fluctuation is a big obstacle in the KLL method, whereas our method is much less subject to the problem.

3.2. Hα CENTERLINE OBSERVATIONS

Figure 2(a) shows one of nine images of a quiet area near disk center taken at the Hα centerline. The light near the upper and right edges was blocked by the field stop. We have processed the image data excluding this blocked region, since the light level in the region is too low to carry information good enough for image

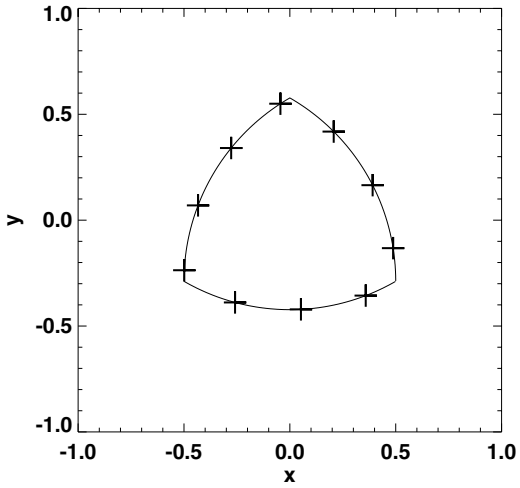

Figure 3. An example of a Reuleaux triangle constructed from an equilateral triangle whose side length is 1. An example of the dither pattern with $N_f = 10$ based on this Reuleaux triangle is represented by the plus symbols.

processing. Figures 2(b) and 2(d) shows the flat pattern and the object image determined from the Hα centerline image data. By default the region excluded in the data processing is set to the median values. In these Hα centerline observations, the root-mean-square contrast of the flat pattern is 4.0% of the mean value and that of the object image is 8.7%. Note the object image in Figure 2(d) has higher signal-to-noise ratio than the single flat field corrected image in Figure 2(c).

4. Performance Test

In this section, we evaluate the performance of our method, especially in comparison with KLL's method.

4.1. Qualitative comparison with KLL's method

Our method may look more complex than the KLL approach. But it has some advantages over the KLL method. It can deal with the situation where either the overall intensity c_k changes from frame to frame, or the input values of displacements are not accurate enough so that they need to be improved. Moreover, our method produces not only the flat pattern, but also the object image as the output.

4.2. SIMULATED DATA

We use simulated data for this test. Construction of simulated data is done in the following steps. We choose $N_x \times N_y$ as the format of the simulated data. We take the central $N_x \times N_y$ pixel region of the flat image in Figure 1 as the input flat image for the data construction.

Then we choose a 'dither pattern', that is, the spatial distribution of the relative displacements (x_k, y_k). It is important to avoid common multiples among the displacements in the dither pattern (Kuhn, Lin, and Loranz, 1991) which may introduce a geometric artifact. There is an infinite number of choices for the dither pattern to satisfy this condition. For our test we choose the Reuleaux triangle (e.g., Arendt, Fixsen, and Harvey Moseley, 2000), which was shown to have good merits for the dither pattern. This kind of dither pattern is characterized by two free parameters: the side length of the basis triangle L and the number of points N_f. Figure 3 presents an example of a 10-point dither pattern constructed from the Reuleaux triangle of $L = 1$.

Next we set c_k to random numbers whose mean and standard deviation are expected to be unity and a small fraction of unity, respectively. The noise n_{ij}^k is similarly set to random numbers whose mean and standard deviation are expected to be zero and a small fraction of unity, respectively. Finally we construct the simulated data a_{ij}^k using Equation (2).

The free parameters to be used in the construction of the simulated data are the number of images or the number of points in the dither pattern (N_f), the size of the dither pattern (L), the standard deviation of the light level change σ_c and the standard deviation of the noise (σ_n). We use the fixed values $N_x = N_y = 512$ for the test. The standard error in the flat pattern, which is of our interest for now,

$$\epsilon = \sqrt{\frac{\sum_{ij}(f_{ij}^{\text{out}} - f_{ij}^{\text{in}})^2}{N_x N_y}}, \tag{17}$$

can be correctly determined since both the input f_{ij}^{in} and the output f_{ij}^{out} are known.

4.3. COMPUTING TIME

In our method the computing time for a single iteration is proportional to $N_x N_y N_f$. In contrast, the computing time in KLL's method is proportional to $N_x N_y N_f^2$. Thus when many frames are used, our method is superior to KLL's method in saving computer time. This characteristic is demonstrated in Figure 4.

4.4. CONVERGENCE AND ACCURACY

Figure 5 shows how the iterative solution converges toward the true solution in the case where $\sigma_c = 0$, $\sigma_n = 0.001$, $L/N_x = 0.2$, $N_f = 10$. The input values x_k

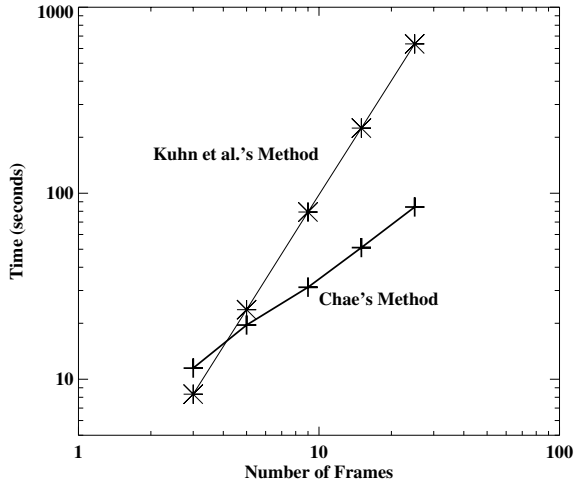

Figure 4. The dependence of the computing time of 10 iterations on the number of image frames. The images are 512 × 512 format.

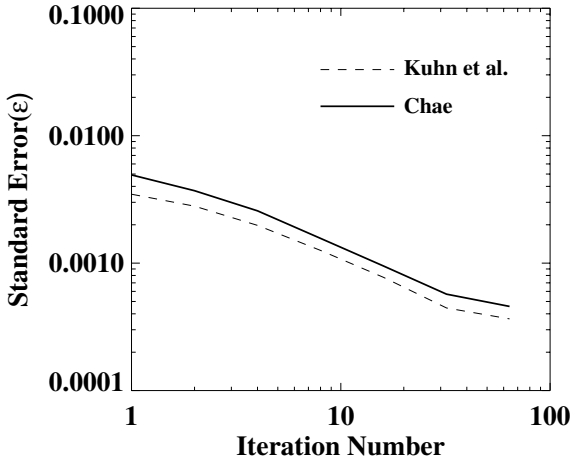

Figure 5. The convergence of the iterative solution in the case the overall intensity remains constant.

and y_k have been rounded off so that the image shifts are to be done by integer multiples of pixels. For future reference we explicitly provide the coordinates of the resulting points of the dither pattern in pixel unit: (50,−14), (40,17), (21,43), (−5,56), (−28,35), (−44,7), (−51,−24), (−27,40), (5,−43), (37, −36). Moreover, we assume that the output values x_k and y_k are correctly known in advance by simply identifying them with these model input values. Note that this assumption is effective only for this ideal case. In practical situations, the real displacements

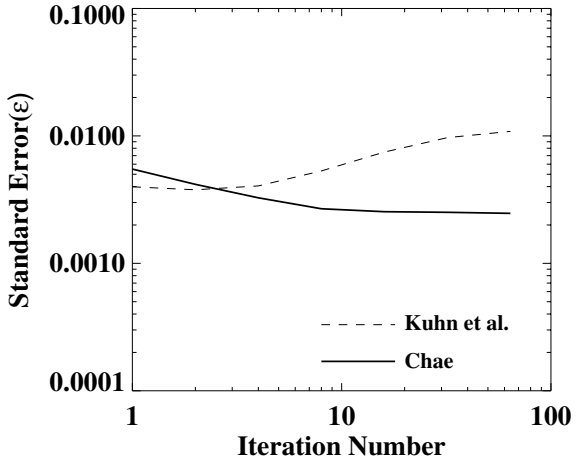

Figure 6. The convergence of the iterative solution in the case the light level changes by 1%.

may be different from the target values because of errors in the telescope pointing and the effect of the seeing. Therefore, the displacements have to be determined self-consistently from the data as described in Section 2.2.

Figure 5 shows that the two methods have very similar convergence patterns in this ideal case, and the KLL method is a little better than our method in accuracy. The difference in accuracy is, however, so small that it may not be significant. After 64 iterations, our method produces a solution with an accuracy of 0.045% and the KLL method produces a solution with an accuracy of 0.035%.

The lower accuracy or the slower convergence in our method may be attributed to the larger number of free parameters to be determined in our method. In the present case we have set c_k, x_k, and y_k to be fixed in our method, so the number of the free parameters to be determined in our method is $2N_xN_y$ which is double the number of the free parameters to be determined in the KLL method.

4.5. Effect of light level variation

When the overall brightness changes with time, the two approaches may produce totally different results as illustrated in Figure 6. In this case we set $\sigma_c = 0.01$ keeping all the other parameters to be the same as above. Note that the implied light level change is very small (1%), which may often arise in real observations, for example, by seeing variations. In our method c_k is treated to be the free parameters to be determined.

Figure 6 shows that the KLL's iterative solution diverges from the true solution when the light level changes. This kind of divergence or low accuracy of the final solution arises because the light level change from frame to frame leads to a spatial gradient in the solution (Kuhn, Lin, and Loranz, 1991). To minimize this effect,

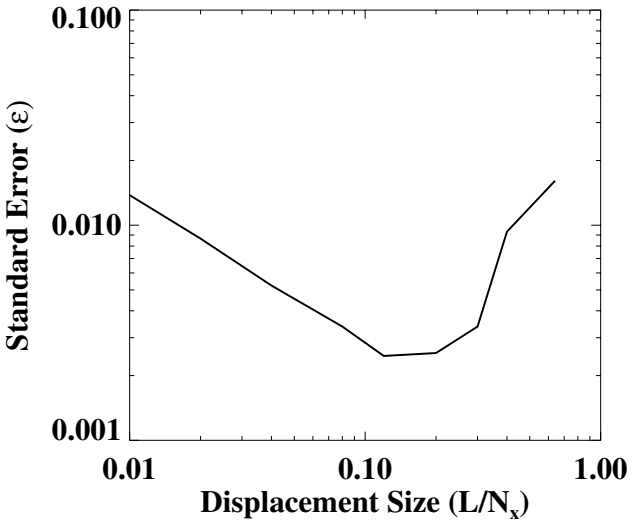

Figure 7. Dependence of the standard error on the characteristic size of the relative displacements.

one may suggest to correct the data by dividing each frame by the corresponding mean or average value so that they have the same mean intensity before the KLL method is applied. This correction, however, is not effective. The mean or median brightness of the data does not correctly reflect the light level since the image data have slightly different fields of view and are affected by the non-uniform flat pattern. Very small amounts of light level change remaining in the corrected data may be still serious in the iteration as seen in Figure 6.

Figure 6 also shows that our method is subject to the same problem, too. But the problem is much less serious in our method than in the KLL method since the light levels in our method are self-consistently determined from the iteration itself. It is obvious that the ability to handle light level change puts a practical limit on the accuracy. In our method it is found to be about 0.25%, which can be achieved after 20 iterations. It is found from experiments that this accuracy is nearly insensitive to the amount of light level change σ_c.

4.6. Dependence on displacement size

Figure 7 presents the effect of L/N_x on the standard error. For these results, we used $\sigma_c = 0.01$, $N_f = 10$, $\sigma_n = 0.001$. The input displacements x_k and y_k have been rounded off in the construction of the simulated data. Unlike the ideal situation above, from now on the output displacements are treated to be free parameters to be self-consistently determined from the data. Therefore a part of the standard error may come from the uncertainty in determining these values. The figure shows that the optimum choice of L/N_x is from 0.10 to 0.25. Too small values of L may

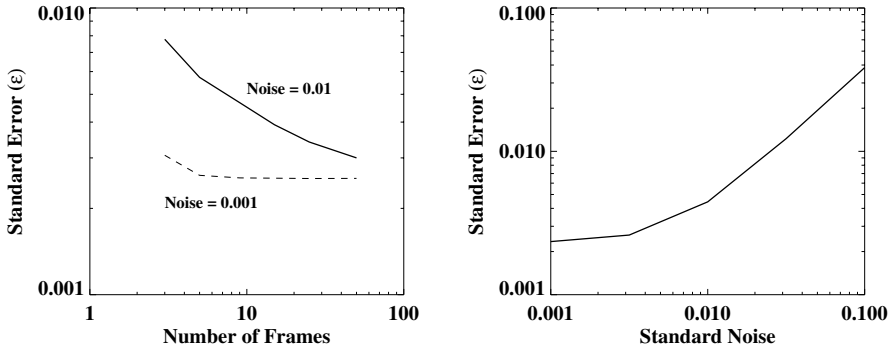

Figure 8. Dependence of the standard error on the number of frames (*left*) and noise (*right*).

lead to a deficiency of low-frequency information in the flat pattern, and too big values of L may result in serious errors in determining the relative displacements, and the reduction of overlapped pixels.

4.7. Dependence on number of frames and noise

The left panel of Figure 8 shows the dependence of the standard error on the number of frames N_f and the noise σ_n. If the noise level in the data is $\sigma_n = 0.001$, the dependence on N_f is weak for $N_f \geq 5$. Thus a small number of frames is enough. On the other hand, when the data contain higher noise ($\sigma_n = 0.01$), more frames produce better results. To attain accuracy in the case $\sigma_n = 0.01$ that is comparable to the case $\sigma_n = 0.001$, more than fifty frames are required.

The right side of Figure 8 shows the dependence of the standard error on noise in the case $N_f = 10$ and $L = 0.2N_x$. The accuracy of the solution is, for example, 0.0025 when $\sigma_n = 0.001$ and 0.0045 when $\sigma_n = 0.01$.

5. Summary

A new method has been presented to determine the flat pattern from a set of relatively shifted images of a non-uniform object. Unlike the method of KLL we simultaneously determine the flat pattern, the object image, the light level change, and the image displacements.

We have found that the method successfully works in real Hα observations. It has been demonstrated from the performance test that our method is superior to KLL's method in computing time and the ability to handle light level variation. The dependence of the iterative solution on the iteration number, the noise level, the size of the dither pattern, the number of points in the dither pattern (that is, the number of frames) has been examined in detail. As a result we found that the

optimal size of the dither pattern is from 10% to 25% of the image size. A solution with an error less than 0.25% can be obtained using our method after about 20 iterations in the typical case with low noise ($N_f = 10$, $\sigma_n = 0.001$, $L = 0.2N_x$).

Acknowledgements

I would like to thank the Big Bear Observatory's observing staff and Hyung Min Park for assistance in the observations, and Yong-Jae Moon and the referee Jeff Kuhn for helpful comments on the manuscript. This work was supported by the Korea Research Foundation Grant (KRF-2002-015-CS0020).

Appendix A. KLL's Iterative Solution

$$F_{ij}^{o} \equiv \frac{\sum_{k,h<k}\left[\left(A_{ij}^{k} - A_{i-x_k+x_h,\,j-y_k+y_h}^{h}\right) w_{ij}^{kh} + \left(A_{ij}^{h} - A_{i-x_h+x_k,\,j-y_h+y_k}^{k}\right) w_{ij}^{hk}\right]}{\sum_{k,h<k}\left[w_{ij}^{kh} + w_{ij}^{hk}\right]}, \quad (18)$$

$$w_{ij}^{kh} \equiv w(i - x_k + x_h,\, j - y_k + y_h), \quad (19)$$

$$\Delta F_{ij} = F_{ij}^{o} - F_{ij} + \frac{\sum_{k,h<k}\left[F_{i-x_k+x_h,\,j-y_k+y_h} w_{ij}^{kh} + F_{i-x_h+x_k,\,j-y_h+y_k} w_{ij}^{hk}\right]}{\sum_{k,h<k}\left[w_{ij}^{kh} + w_{ij}^{hk}\right]}. \quad (20)$$

References

Arendt, R.G., Fixsen, D. J., and Harvey Moseley, S.: 2000, *Astrophys. J.* **536**, 500.
Dalrymple, N. E., Bianda, M., and Wiborg, P. H.: 2003, *Publ. Astron. Soc. Pacific* **115**, 628.
Denker, C., Johannesson, A., Marquette, W., Goode, P. R., Wang, H., and Zirin, H.: 1999, *Solar Phys.* **184**, 87.
Fixsen, D. J., Moseley, S. H., and Arendt, R. G.: 2000, *Astrophys. J. Suppl.* **128**, 651.
Kuhn, J. R., Lin, H., and Loranz, D.: 1991, *Publ. Astron. Soc. Pacific* **103**, 1097.
Stetson, P. B., and Harris, W. E.: 1988, *Astron. J.* **96**, 909.
Wild, W.: 1997, *Publ. Astron. Soc. Pacific* **109**, 1269.
Yang, G., Xu, Y., Wang, H., and Denker, C.: 2003, *Astrophys. J.* **597**, 1190.